Macromolecules
ARTICLE

Macromolecules **2010**, *43*, 7173–7184 **7173**
DOI: 10.1021/ma100744p

^{2}H NMR and Simulation Studies of Chain Segment Orientation in PDMS Bimodal Networks

Bernardo M. Aguilera-Mercado,† Geoffrey D. Genesky,† T. Michael Duncan, Claude Cohen, and Fernando A. Escobedo*

School of Chemical and Biomolecular Engineering, Cornell University, Ithaca, New York 14853.
† *These authors contributed equally to this work.*

Received April 6, 2010; Revised Manuscript Received July 27, 2010

ABSTRACT: We present a systematic study through ^{2}H NMR and molecular simulations of chain segment orientation in model PDMS bimodal networks. Estimates of the average segment orientation order parameter in model PDMS bimodal networks compare well to those of equivalent simulated networks. We find that line shapes of short and long chains are different due to the dissimilar degrees of motional restrictions. Short-chain conformations are perturbed from random coiled states when incorporated into bimodal networks whereas long-chain conformations are unaffected. Although experiments and simulations both indicate that the overall segment orientation normalized by the elastic modulus is fairly constant across all bimodal network compositions, short-chain normalized segment orientation displays a nonmonotonic trend with the network composition (related to changes in network microstructure and mechanical properties). Finally, we show that the unusual outer splittings observed in spectra of highly extended unimodal and bimodal samples correspond to segments in long chains able to be exceptionally stretched and oriented along the strain axis.

1. Introduction

Bimodal polymer networks have attracted interest due to their interesting mechanical properties.[1] These elastomers are synthesized from chemically identical telechelic chains of two different molar masses. When these precursor chain lengths are widely separated, the end-linked networks require increased energy to rupture (toughness) and stress increases markedly at high elongation.[2] The connection between these interesting macroscopic properties and the conformations of the network chains has long been a matter of debate. For instance, some researchers have claimed that the short chains cluster into heterogeneous domains which could toughen networks, like filler particles toughen commercial rubbers.[3,4] The ability of short chains to segregate in such systems has been confirmed using a variety of methods,[3,5−7] but a connection between this microstructure and an enhancement in mechanical properties has not been demonstrated. Others have attributed the improved mechanical properties of bimodal networks to the finite extensibility of the short chains when the network is highly elongated.[2,8−10] In this hypothesis, the highly stretched short chains increase the stress abruptly, while the more moderately extended long chains allow the network to strain highly before fracturing.

Studies of chain segment orientation with increasing elongation ratio α are valuable in illuminating structure−property relationships in bimodal networks. ^{2}H NMR is a powerful method to investigate these network properties at local scales because the NMR frequency spectrum $f(\nu)$ is determined by the distribution of the chain segment orientation order parameter S. In the polydimethylsiloxane (PDMS) chains studied here, the CH_3 side groups are selectively replaced by $C(^2H)_3$ groups. Chain segment orientation is monitored through the deuterium quadrupole interaction between the electrostatic field gradient along the labeled C−^{2}H bonds. The resulting line shape of an unstrained elastomer is broader than the line shape of a melt but much narrower than that of a rigid solid. As the network is uniaxially extended, motional averaging of the quadrupole interaction is constrained due to the anisotropic orientation of chain segments, and the spectra broaden. The line shape eventually forms two symmetric peaks (which represent the most frequently accessed degree of time-averaged segment orientation) separated by distance $\Delta\nu$. Both experiments and models have shown that these peaks result from interchain excluded volume interactions.[11−14]

Given the interest in the structure and properties of bimodal networks and the ability of ^{2}H NMR experiments to monitor either the short or long chains through selective labeling, relatively few ^{2}H NMR studies have been performed on this type of elastomer. Chapellier et al.[15,16] and Sotta[17] selectively labeled 3000 and 25 000 g/mol PDMS chains and monitored the peak splittings $\Delta\nu$, concluding that the short- and long-chain segments experienced similar orientation with increasing strain. However, bimodal networks have been found to display enhanced mechanical properties only when the precursor molar masses differ by at least a factor of 10.[8,9] The relatively small ($\sim$8$\times$) difference in molar masses employed by these authors may have not been sufficient to correlate segmental orientation with macroscopic properties in bimodal elastomers.

Other experimental methods have also been used to probe chain segment orientation in bimodal networks. Stress-optical studies have noted nonlinearity in plots of birefringence vs stress.[18−20] This effect becomes more pronounced with increasing short-chain concentration, suggesting changes in spatial heterogeneity with composition.[19] Infrared dichromism studies have found a similar degree of segment orientation for the short and long chains in polytetrahydrofuran networks[21] but an increased ordering for the short chains when they occupy a majority of the volume of a bimodal PDMS network.[22] Monte Carlo (MC) simulations have also found a higher degree of segmental order.[23] More recently, multiple quantum (MQ) NMR has been utilized

*Corresponding author. E-mail: fe13@cornell.edu.

Published on Web 08/12/2010

to elucidate the distribution function of local chain order in elastomers.[24] This method reveals that the distribution has two components for bimodal networks in the unstretched state,[7,25] suggesting a heterogeneous structure brought about by the differences in precursor chain lengths. However, MQ-NMR spectroscopy has yet to be applied to uniaxially stretched bimodal networks to monitor chain segment orientation of each component with strain.

Herein we present a systematic study, through ^{2}H NMR and molecular simulations, of chain segment orientation in model PDMS bimodal networks. These well-characterized elastomers contain selectively deuterated short or long chains to monitor the degree of chain segment orientation of each component in both the unstrained and highly stretched states. Although the spectra for stretched networks split into two peaks symmetric around $\nu = 0$, the segment orientation is not well described by these peak locations.[26] Therefore, we utilize a recently developed theoretical strategy[27] to estimate the average frequency $\langle\nu\rangle$ from ^{2}H NMR spectral data for both short and long chains upon uniaxial extension. The ensemble average frequency $\langle\nu\rangle$ is over the frequency probability distribution, rather than the ^{2}H NMR spectrum, and is directly proportional to the average segmental alignment; this average frequency $\langle\nu\rangle$ describes more accurately (than solely the frequency splittings $\Delta\nu$) the widening of the line shape and the overall segment orientation.[27] Estimates of the average segmental alignment $\langle\nu\rangle$ in model PDMS bimodal networks are compared to averages of segmental order $\langle S\rangle$ in roughly equivalent simulated bimodal elastomers. Variations in the ^{2}H NMR response at different bimodal compositions are closely related to changes in the network microstructure and the resulting macroscopic mechanical properties. Additionally, we investigate in more detail ^{2}H NMR spectra of unimodal and bimodal samples uniaxially stretched to high extension ratios that exhibit a peculiar shoulder in the line shape, that is, two characteristic quadrupolar splittings;[28] through molecular simulations we explore the microstructural nature of these unusual two splittings.

Table 1. Network Compositions and Properties

5000(^{2}H)−80000 g/mol Bimodal Networks

mol % short chains	Q	E (MPa)	w_{sol} (mass %)	$\langle\|\nu\|\rangle_0$ (Hz)	q^a (Hz/MPa)
60	4.76	0.59	1.72	193	31.1
70	4.53	0.64	1.49	205	66.6
80	4.21	0.73	1.61	209	56.3
90	3.65	0.93	0.88	260	81.5
95	3.26	1.14	1.13	282	112.0
98	3.17	1.20	1.92	230	

5500−90000(^{2}H) g/mol Bimodal Networks

mol % short chains	Q	E (MPa)	w_{sol} (mass %)	$\langle\|\nu\|\rangle_0$ (Hz)	q^a (Hz/MPa)
60	5.24	0.49	2.18	81	71.6
70	4.68	0.60	1.82	89	72.0
80	4.09	0.76	1.01	85	71.9
90	3.99	0.80	2.31	84	65.2
95	3.78	0.88	2.46	87	49.9

Unimodal Networks

M_n (g/mol)	Q	E (MPa)	w_{sol} (mass %)	$\langle\|\nu\|\rangle_0$ (Hz)	q^a (Hz/MPa)
5 000	3.02	1.30	0.59	181	54.5
11 000	3.39	1.06	0.80	169	93.3
36 000	4.64	0.61	1.45	96	65.0
90 000	7.31	0.27	5.48	77	106.5
30 000[b]	4.55	0.63	2.36	47	26.3
36 000d[c]	5.98	0.39	1.46	107	73.3
36 000p[c]		0.35[d]		103	80.6

[a] q = slope of best fit line through $(\langle\nu\rangle/E)/(\alpha^2 - 1/\alpha)$. [b] Consists of unlabeled elastic chains and ^{2}H-labeled probe chains, both with M_n = 30 000 g/mol. Unlabeled soluble material was extracted before dissolution of labeled free chains. [c] Unimodal network made with 70 mass % 36 000 g/mol ^{2}H-labeled precursor chains and 30% 2000 g/mol nonreactive and unlabeled "solvent" chains. ^{2}H NMR experiments were performed on networks in the prepared state (p) and in the dry state after extraction of the solvent chains (d). [d] Elastic modulus of network in the prepared state calculated from E of the dry network as detailed in the text.

2. Procedures

2.1. Experimental Procedures. Both hydrogenated and randomly deuterated PDMS precursor chains were synthesized using methods detailed in an earlier publication.[29] Number-average molar masses were determined to be 5500 (^{1}H), 80 000 (^{1}H), 5000 (^{2}H), and 90 000 (^{2}H) g/mol by gel permeation chromatography (GPC). These chains were combined into 5000−80 000 and 5500−90 000 g/mol selectively labeled bimodal blends at the desired compositions (60−98 mol % short chains). We also used 11 000 (^{2}H), 30 000 (^{1}H, ^{2}H), and 36 000 (^{2}H) g/mol chains to synthesize unimodal networks. The polydispersity index of all chains was 1.32 or lower. For both unimodal and bimodal networks, tetrakis(dimethylsiloxy)silane cross-linker was added such that the ratio of cross-linking arms to polymer chain ends was 1.7 to form networks of the highest possible quality.[30] Because this optimal ratio is smaller for shorter precursor chains,[31] it was reduced to 1.5 for the 5000 g/mol unimodal sample only. In one network, 36 000 g/mol chains were mixed with nonreactive 2000 g/mol chains at a 70/30 mass % ratio before cross-linking. This network was tested in the preparation state (36 000p) and in the dry state after extraction of the free chains (36 000d). The PDMS/cross-linker mixtures were well-stirred with a spatula and mixed on a rotator overnight for homogeneous distribution of the components. Networks were formed upon addition of the catalyst *cis*-dichlorobis-(diethyl sulfide)platinum(II) using the methods detailed in ref 29. Equilibrium mass swell Q, soluble fraction w_{sol}, and elastic Young's modulus E of the fully cured elastomers were all determined by previously reported techniques.[29] The E value for 36 000p was calculated from that of 36 000d by multiplying the latter by the polymer volume fraction in the prepared state raised to the 1/3 power.[32] These bimodal and unimodal network properties are reported in Table 1. ^{2}H NMR data were obtained on a Tecmag Apollo HF spectrometer operating at 30.72 MHz for deuterium by employing a 5 μs 90° pulse. For stretched samples, the direction of the magnetic field is perpendicular to the strain axis. Methods for processing these data are described in ref 28.

2.2. Estimating the Average Chain Segment Order $\langle\nu\rangle$ from ^{2}H NMR Spectra. In this paper we used a recent theoretical method[27] that estimates, from ^{2}H NMR spectral data, the average frequency splitting $\langle\nu\rangle$ or segment-orientation order parameter of chain segments in a polymer network. Calculation of $\langle\nu\rangle$ is valuable to understand chain segment alignment because the observed quadrupolar splitting $\Delta\nu$ does not measure the total average orientation of the chain segments. Several works[11−14] have shown that the quadrupolar splitting $\Delta\nu$ induced at high elongation measures only segment orientation resulting from excluded volume interactions between interacting chains. Conversely, the average frequency $\langle\nu\rangle$ accounts for the segment orientation resulting from both excluded volume interactions and constraints imposed by the cross-links along with chain entanglements within a given network. However, the ensemble average frequency $\langle\nu\rangle$, defined by eq 1a, cannot be calculated directly from spectral data because the ^{2}H NMR frequency spectrum $f(\nu)$ is the

Table 2. Characteristics of the Simulated Set of Unimodal Networks

chain length (no. of beads)	r_x	no. of chains	no. of cross-links	w_{sol} (mass %)	inelastic cont (mol %)	slope q[a]
15	1.05	1659	871	0.00	5.3	0.339
29	1.10	858	472	0.00	4.4	0.341
43	1.05	579	304	0.00	3.3	0.343
129	1.15	193	111	0.00	2.6	0.357

[a] Slope q is the average slope of the plot $\langle S\rangle/E$ vs $\alpha^2 - 1/\alpha$ and is in $\sigma_{LJ}{}^3/k_BT$ units.

Table 3. Characteristics of the Simulated Set of (15−300-Bead) Bimodal Networks

short chain cont (mol %)	r_x	no. of short chains	no. of long chains	no. of cross-links	w_{sol} (mass %)	inelastic cont (mol %)	total slope q[a]
60	1.15	110	73	105	0.07	25.1	0.344
70	1.00	169	73	121	0.13	18.2	0.330
80	1.10	268	67	185	0.25	15.8	0.331
90	1.05	490	54	286	0.00	12.7	0.319
95	1.10	778	41	451	0.00	9.3	0.313
98	1.10	1106	21	621	0.07	7.5	0.315
100	1.05	1659	0	871	0.00	5.3	0.339

[a] Total slope q (in $\sigma_{LJ}{}^3/k_BT$ units) is the slope of the plot $\langle S\rangle/E$ vs $\alpha^2 - 1/\alpha$ where $\langle S\rangle$ is the weighted average chain segment order parameter of short and long chains.

frequency probability distribution $\rho(\nu)$ symmetrized around $\nu = 0$ (eq 1b), and all the odd moments of $f(\nu)$ are therefore equal to 0.[27] On the contrary and due to this symmetric relationship between $f(\nu)$ and $\rho(\nu)$, their even moments and the average absolute values of any power of ν are identical for both $f(\nu)$ and $\rho(\nu)$ (eq 1c).[27]

$$\langle \nu \rangle = \int \nu \rho(\nu)\, d\nu \tag{1a}$$

$$f(\nu) \propto \rho(\nu) + \rho(-\nu) \tag{1b}$$

$$\langle |\nu| \rangle = \int \rho(\nu)|\nu|\, d\nu = \frac{\int f(\nu)|\nu|\, d\nu}{\int f(\nu)\, d\nu} \tag{1c}$$

where $f(\nu)$ is the ^{2}H NMR signal at frequency ν, $\rho(\nu)$ is the probability density distribution of frequencies ν, and the integrals are over the entire frequency spectrum.

The employed strategy[27] to estimate $\langle \nu \rangle$ is based on truncated Taylor expansions and considers the entire ^{2}H NMR line shape, including the wide spectral wings often observed for elastomers. After computing the average absolute value $\langle |\nu| \rangle$ from eq 1c,[27] the estimate of the average frequency $\langle \nu \rangle$ (or average segment orientation order parameter) for uniaxial extension is solved for from the following nonlinear equation:[27]

$$\frac{\langle |\nu| \rangle}{\langle |\nu| \rangle_0} \cong \frac{\langle \nu \rangle}{\langle |\nu| \rangle_0} + \exp\left(-\frac{\langle \nu \rangle}{\langle |\nu| \rangle_0}\right) \tag{2}$$

where $\langle |\nu| \rangle_0$ is the average absolute frequency value of the unstrained sample.

2.3. Simulation Procedures. ^{2}H NMR spectral data were calculated for coarse-grained bimodal networks obtained from Monte Carlo simulations. In our previous work[29] we have shown that the molecular model used in this work provides a good representation of model PDMS bimodal networks in terms of mechanical properties and network microstructure. The simulation methods for the end-linking reaction, uniaxial deformation, and obtaining the ^{2}H NMR spectrum of the simulated networks are briefly described below. A more comprehensive description of these simulation procedures can be also found in ref 29.

2.3.1. Network End-Linking. The end-linking reaction was simulated on a lattice using the bond fluctuation model (BFM).[33] In this scheme, coarse-grained cubes representing chain monomers and cross-links are capable of forming chemical bonds along any of 108 bond vectors accessible in the BFM. Each coarse-grained unit roughly mimics four monomers of PDMS (~300 g/mol).[29] The simulation of the end-linking reaction is carried out athermally; that is, only bonding restrictions and excluded-volume interactions were considered. For all the simulated networks, lattice volume fractions were set around 0.47, resembling meltlike conditions.[34] Hop moves, which mimic diffusive dynamics,[35] of the coarse-grained cubes were used to equilibrate polymer chains and cross-links. This equilibration stage involved 10^6 moves per coarse-grained unit on average.

The end-linking reaction was initiated after equilibration, by allowing bond formation between chain ends and cross-links, as the system relaxed through the hop moves. When the fraction of unreacted chain ends was 0.01 or lower, the reaction was ended. The resulting soluble mass fractions were less than 0.003, and the mole fractions of inelastic chains (single looped or pendant) were no greater than 0.05 in the unimodal networks and 0.25 in the bimodal networks. The ratio of cross-link arms to chain ends, r_x, was used to tune the soluble fraction for each simulated network. Detailed information about the resulting simulated networks is shown in Tables 2 and 3.

2.3.2. Network Uniaxial Deformation. Uniaxial extension, NPT Monte Carlo simulations were conducted off-lattice to produce continuous and smooth deformations. Preserving the network structure and polymer volume fraction, coordinates from the end-linking (on-lattice) simulations were transformed into a continuous framework. In this continuous scheme, coarse-grained units that represent chain monomers and cross-links were modeled as purely repulsive beads, through a cut-shifted Lennard-Jones interaction potential, with diameter σ_{LJ} and interaction energy ε_{LJ}. An infinite square-well potential was used to model the interaction between bonded beads; such bonding potential allowed bond lengths to fluctuate between $0.8\sigma_{LJ}$ and $1.2\sigma_{LJ}$.

One Monte Carlo cycle consisted of a fixed number (equal to the total number of beads in the system) of attempted single-site moves (95% hops and 5% flips) plus two volume moves in complete random order. Hop, flip, and volume moves had acceptance ratios of 0.30, 0.45, and 0.35, respectively. Simulations were performed at temperature $T = 2.0$ (in ε_{LJ}/k_B units), pressure $P = 3.0$ (in $k_BT/\sigma_{LJ}{}^3$ units) at the unperturbed state, and the resulting meltlike density was

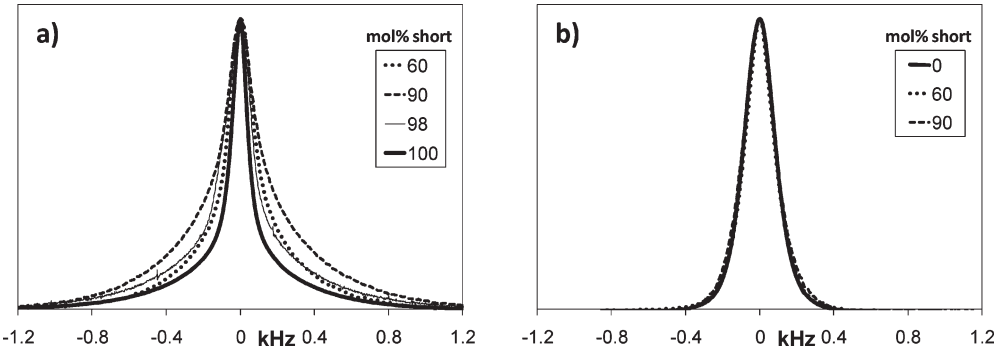

Figure 1. ^{2}H NMR spectra for (a) short (5000 g/mol) and (b) long (90 000 g/mol) chain segments in bimodal networks. Spectra are measured on samples in the unstrained state and are normalized by peak height.

$\sim$0.8 (in $1/\sigma_{LJ}^3$ units). An isostress ensemble was employed to simulate the deformation of the networks subject to given stresses. The imposed stresses on the z direction are the result of the differences of applied normal stresses $(P_{xx} + P_{yy})/2 - P_{zz}$, where P_{xx}, P_{yy}, and P_{zz} are the applied normal stresses in the x, y, and z directions, respectively, and the quotient of the box z-length after equilibrating the system for a given stress to the initial undeformed box z-length gives the extension ratio α. On average, the box dimensions reached plateau values (i.e., the system achieved mechanical equilibrium) after 10^7 Monte Carlo cycles.

2.3.3. Simulated ^{2}H NMR Spectra. If the chain segments are in "the fast motion limit" (i.e., when the temperature is higher than the polymer glass transition temperature), the ^{2}H NMR spectrum $f(\nu)$ can be written as the symmetric part of the frequency (or order parameter) distribution $\rho(\nu)$;[36] that is, $f(\nu) \propto \rho(\nu) + \rho(-\nu)$. Hence, simulated spectra can be extracted straightforwardly from the order parameter distributions obtained from Monte Carlo simulations.[36−38] Because $\rho(\nu)$ is the distribution of the time-averaged segment-orientation order parameter, values of order parameter for each chain segment were stored every 40 cycles during an additional run of $\sim 3 \times 10^7$ cycles. This additional run was performed after the deformed networks reached equilibrium. Subsequently, the average order parameter over the entire additional run is computed for each chain segment and used to construct the distribution histogram of the order parameter $\rho(\nu)$. The simulated frequency spectrum $f(\nu)$ was obtained by normalizing $\rho(\nu) + \rho(-\nu)$. The width of the bins used to construct the histograms ranged between 0.002 and 0.004 in order parameter (dimensionless) units for all the simulated systems.

3. Results and Discussion

3.1. Unstrained Bimodal Networks. ^{2}H NMR spectra for undeformed bimodal networks with selectively labeled short and long chains are shown in Figures 1a and 1b, respectively. All spectra are plotted with equal peak heights to emphasize the relative contributions from the center portion of the line shape and the high-frequency spectral wings. Comparison of Figures 1a and 1b demonstrates the different line shape characteristics for the 5000 and 90 000 g/mol chains. While the short-chain spectra have wide wings that form the "super-Lorentzian" shape typically observed for PDMS networks,[39,40] the long-chain line shapes are relatively broad in the center but diminish rather quickly. Because the spectral wings correspond to the portion of the segment order distribution that is associated with more highly stretched chains, we have attributed the 5000 g/mol line shape to a higher proportion of these chains cross-linked when they were in a conformation with relatively higher radii of gyration. This is more clearly observed in Figure 2a, where only the distributions of the radius of gyration for the elastic short chains in the simulated networks are displayed. As shown in Figure 2a, the elastic short chains in the bimodal networks shown (60 and 90 mol % short) are slightly more stretched than those in a network of pure short chains (100 mol % short). This is because the cross-links are effectively farther apart in bimodal networks where they are less concentrated than in networks made of pure short chains, and as a consequence, short chains may need to stretch slightly more to reach them. The long chains, meanwhile, appear to be less perturbed from their melt configurations because the number of accessible cross-links inside their pervaded volume is still very high for all the short chain contents (see values of n_x in Table 4 of ref 29).

Figure 1 reveals that these general line shapes persist for 5000 and 90 000 g/mol chains when they are incorporated into bimodal networks. However, it is immediately clear from Figure 1a that the line shape of the short chain segments evolves with network composition, while the line shapes of the long chains appear unchanged as their concentration varies. The wings increasingly contribute to the spectra as the short-chain content is increased from 60 to 90 mol % and then shrink at 98 mol % and for the unimodal short-chain network (100 mol %). The wider spectral wings observed in the 90 mol % short network, with respect to 60 mol % short network, can be attributed to the fact that the elastic short chains in the 90 mol % network are slightly more stretched than those in the 60 mol % network (Figure 2a). This trend also holds for the labeled short-chain networks (70, 80, and 95 mol %) that were omitted from the figures for clarity.

The varying wing contribution to the spectra is clearly quantified in Figure 2b, where the relative average absolute values at the unperturbed state $\langle|\nu|\rangle_0$ (eq 1c), normalized with respect to $\langle|\nu|\rangle_0$ of the network with 100 mol % of short chains, for short and long chains in the PDMS networks are plotted against mass (and mol) % of short chains. Figure 2c shows the dependence of the relative (dimensionless) average absolute frequency value $\langle|\nu^*|\rangle_0$ with the network composition for the simulated bimodal networks. Error bars in Figure 2c are always smaller than the symbols used; specifically, the uncertainty is on average 0.02 and 0.005 (in dimensionless units) for short and long chains, respectively. Although Figures 2b and 2c differ qualitatively, a much stronger dependence on the network composition of average absolute frequency value $\langle|\nu|\rangle_0$ of the short-chain segments is evident for both experimental and simulated networks. Qualitative discrepancies between experimental and simulated results for $\langle|\nu|\rangle_0$ may be attributed to the fewer defects present in the simulated network models. A maximum $\langle|\nu|\rangle_0$ for the short chains is observed (Figures 2b and 2c) around a network composition of 95 mol % of short chains or $\sim$50−60 mass %

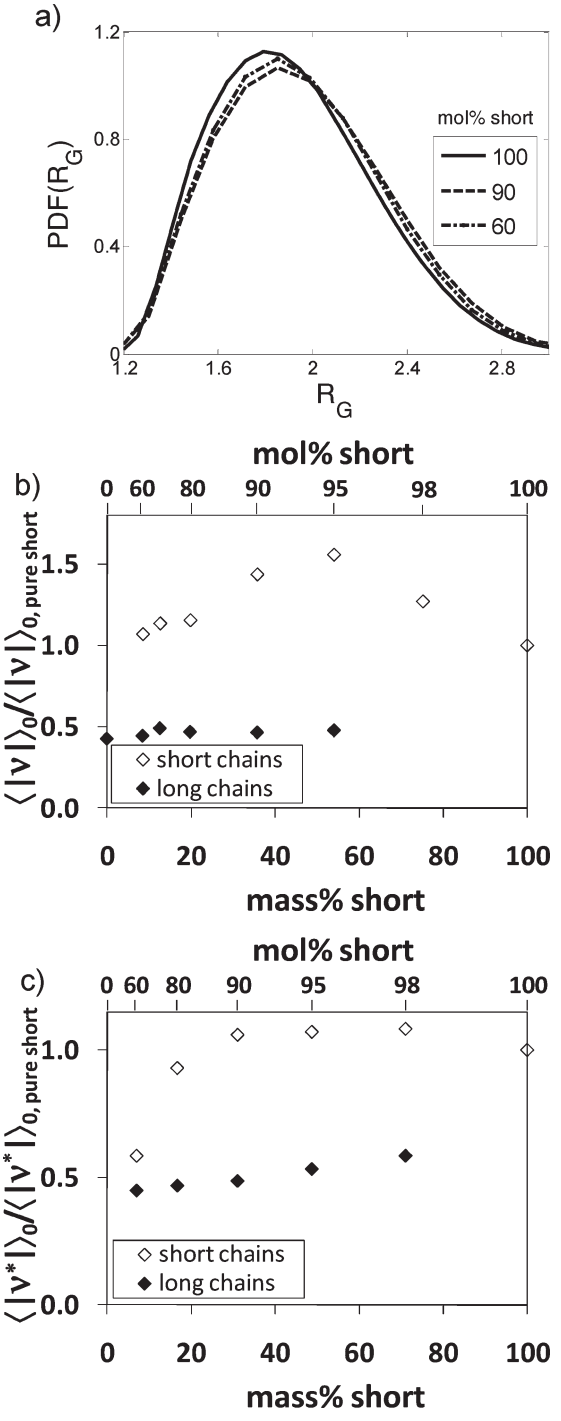

Figure 2. (a) Probability density function for the radius of gyration (in σ_{LJ} units) of elastic short chains only in simulated networks with different short-chain compositions. (b) Experimental and (c) simulation values of the average absolute value for unstretched bimodal networks $\langle|\nu|\rangle_0$, relative to the value of $\langle|\nu|\rangle_0$ for the 100 mol % of short network, with varying short-chain concentration.

of short chains. At this network composition, most short chains would be elastically coupled and would form an infinite cluster that pervades the entire space. Additional work is necessary to confirm this conjecture about the network microstructure at such compositions.

The nearly constant line shape for the long chains in Figure 1b is well described by the constant value of $\langle|\nu|\rangle_0$ across all concentrations in Figure 2b. Thus, the residual segmental order imposed on the long chains during cross-linking is not significantly affected by the introduction of a bimodal distribution of chain lengths. Long chains also showed similar segmental order parameter distributions across a variety of bimodal network compositions in recent MQ-NMR studies of 800−47 000 g/mol PDMS elastomers.[7,25] In unimodal 90 000 g/mol networks, the line shape broadens only slightly upon network formation because the cross-link concentration is low, and the network chains are perturbed negligibly from their random coiled states.[28] Clearly, this persists in bimodal networks even with the increase in cross-linking density caused by the introduction of short chains. The 90 000 g/mol chains likely react with the nearest cross-linker without much change in their melt state segmental order or end-to-end distance. An alternative physical interpretation for these nearly unperturbed line shapes for the long chains may be that the topological constraints imposed on the long chains by the cross-links are not as fixed in space over the time scale of the NMR experiment as they are for short chains. In either case, the impact of the network composition on the line shapes is significantly stronger on the short chains than on the long chains.

The short chains are clearly affected by incorporation into the bimodal network. We believe the variation in the spectral wings to be a consequence of changes in the network topology with short-chain concentration in the network. MC simulations have demonstrated an increased pair distribution function for the intermolecular centers of mass $g(r)$ upon cross-linking for 60 mol % short-chain bimodal networks with molar masses similar to those employed in these experiments.[29] Therefore, the short chains can aggregate into heterogeneous domains when their concentrations are relatively low due to the faster diffusion of the mobile chains and cross-linkers in the mixture. Clustering has also been observed for networks with low short chain concentrations via SANS[3,6] and light scattering.[5] Therefore, it is not surprising that the line shapes for the 60 and 100 mol % short chain networks are similar ($\langle|\nu|\rangle_0$ = 193 and 181 Hz) even though the network compositions are very different. Because the short chains form clusters in the 60 mol % network, most of a given short chain's neighbors are other short chains and the cross-link density in their vicinity is quite high. Thus, the segmental order of these chains is affected negligibly by the presence of the long chains, and the microstructure can be pictured as small domains of 5000 g/mol unimodal network dispersed in a unimodal network of long chains. The similarity of 98 and 100 mol % short-chain spectra, meanwhile, is expected given the similar number of the 5000 g/mol chains in each system. The smaller chains dominate the volume of the network in this bimodal system. Consequently, we suspect the long chains to be intermittently woven into an interconnected skeleton of short chains that spans the whole network. The 90 and 95 mol % networks have the most prominent spectral wings in Figures 1a and 2, indicating a greater degree of motional restriction on their short-chain segments. At these concentrations the short chains are near their overlap concentrations in a 5000−80 000 g/mol system. Thus, it appears that the lower molar mass chains in these networks do not form small clusters, but instead reach cross-linker arms when they are slightly elongated from their random states. Here, the difference in residual segmental order between the short- and long-chain segments is at a maximum (Figure 2b).

3.2. Stretched Bimodal Networks. Both experiments[13] and theoretical models[11,14,26] have established that the quadrupolar splitting $\Delta\nu$ induced at high extension is the result of excluded volume interactions between chain segments. When normalized by the elastic modulus E, $\Delta\nu$ has been shown to follow a universal relationship with the extension

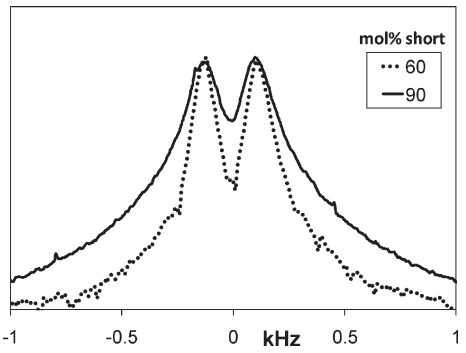

Figure 3. Bimodal networks at 60 and 90 mol % ^{2}H-labeled short chains (α = 2.43 and 1.81, respectively) have similar spectral splitting $\Delta\nu$ but different overall line shapes. The wide spectral wings in the 90 mol % network indicate a large contribution from highly stretched chains.

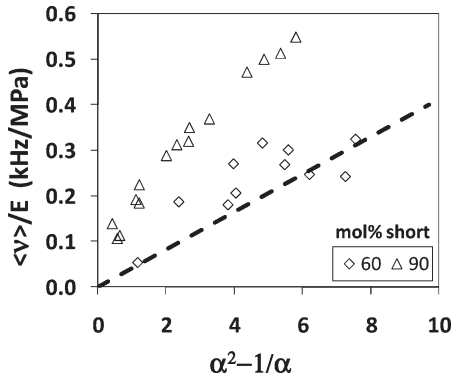

Figure 4. Average segmental order $\langle\nu\rangle$ normalized by elastic modulus E for bimodal networks at 60 and 90 mol % ^{2}H-labeled short chains at increasing extension. The 60 mol % short-chain segments follow approximately the universal curve for excluded volume interactions between chain segments $^1/_2\Delta\nu/E$ (dashed line). The average order is much higher for the short chains in the 90 mol % network due to its wide spectral wings.

term $\alpha^2 - 1/\alpha$.[13] However, additional details of the ^{2}H NMR line shape describe network chains that are greatly affected by the network constraints.[38,26] Specifically, the outer frequency portions of the line shape have been associated with more ordered chain segments that have less motional averaging because these wings represent the tail of the order parameter probability distribution.

Figure 3 further illustrates why the peak frequency split $\Delta\nu$ is not useful as a measure of the average segmental order. Although the short chains in the 60 and 90 mol % networks each have a similar $\Delta\nu$ value in the plotted spectra, the wings are noticeably more prominent in the latter. Therefore, the higher proportion of ordered chain segments found in the rest state for the 90 mol % short chain elastomer (Figure 1a) continues as the network is extended. Clearly, the initial chain conformations affect the segmental order induced upon loading. Because of these differences in line shape, we used eq 2 to calculate the average segmental order $\langle\nu\rangle$ for the 60 and 90 mol % short chain bimodal networks at various elongation ratios. The results are normalized by the corresponding elastic modulus and displayed in Figure 4 against the average segmental order resulting from intersegmental interactions (section 3.3). We must compare to $^1/_2\Delta\nu/E$ here because the two peaks in a ^{2}H NMR spectrum are the result of the order parameter distribution and its mirror image reflected about $\nu = 0$. Although the trend for the 60 mol % short chain sample is noisy due to the lower ^{2}H content in this network, it clearly follows the $^1/_2\Delta\nu/E$ trend more closely than the 90 mol % network. Consequently, the segmental order of short chains in the 60 mol % network is more influenced by excluded volume interactions between segments than by chains with large end-to-end distances.

Because we selectively labeled both the short and long chains in our PDMS bimodal networks, it is instructive to compare the segmental order as each sample is stretched. These plots of $\langle\nu\rangle/E$ vs $\alpha^2 - 1/\alpha$ are displayed for 60, 70, 90, and 95 mol % short-chain networks in Figure 5. The segmental orientation of the short chains approaches and surpasses that of the long chains as the short-chain concentration increases. At 60 mol % short chains, the clustered chains appear to be shielded from order by the more compliant long-chain matrix. We recently concluded that such highly heterogeneous networks do not show enhanced macroscopic properties,[29] and the results in Figure 5a reinforce this view. If short-chain clusters were to aid in the toughening of these elastomers, the short chains would have to sustain a significant portion of the applied load. Instead, the ordering of these segments appears to be highly influenced by interchain segmental interactions (Figure 4).

Analogous results for simulated bimodal networks are displayed in Figure 6, where the dependence of the normalized chain segment order parameter ($\langle S\rangle/E$) on extension ($\alpha^2 - 1/\alpha$) is displayed for 60, 70, 90, and 95 mol % short chains. Simulations predict similar segment orientation for both chains upon uniaxial extension of a 60 mol % short-chain network (Figure 6a) whereas this equivalence occurs experimentally when the short-chain content is 70 mol % (Figure 5b). Therefore, the agreement between simulations and experiments is reasonable. The discrepancy in the equivalence point may be attributed to small variations in the microstructure of simulated networks caused by different cross-link concentrations employed in curing simulations (~30% lower than in experiments). Lower cross-link concentrations were used in the BFM end-linking simulations because they yield nearly ideal networks with very low (~0.1 mass %) minimum soluble fractions at such concentrations.[29,41] Beyond this equivalence point in segmental orientation between short and long chains, segments on the shorter chains are more aligned than those from the long chains.

The results for the simulated 90 and 95 mol % short chain networks (Figures 6c and 6d) slightly differ from trends observed in the experimental networks (Figures 5c and 5d). However, short-chain segments orient significantly more than long chain segments in both experimental and simulated networks with short chain content of 90 and 95 mol %. Contrary to the experimental evidence, in simulated networks short-chain segments orient more upon extension in the 90 mol % network than in the 95 mol % network. The disparity of the observed trends may imply, as aforementioned, the existence of certain differences in microstructural details between (experimental) PDMS and simulated networks. Nevertheless, a perfect mapping (as a function of network composition) between the microstructures of experimental and simulated networks should not be expected because the used coarse-grained molecular model is very simple and lead to more perfect structures than can be achieved experimentally, as previously mentioned in section 3.1.

Networks at 90−95 mol % short chains display the greatest enhancement in mechanical properties[2,8,9,29] because further addition of short chains leads to very brittle samples. Note that even the 95 mol % short chain network breaks at a small value of α (Figure 5d). Increased ordering of the short chain segments appears to play a role in generating the stress upturn at high strain and increased toughness of these networks.

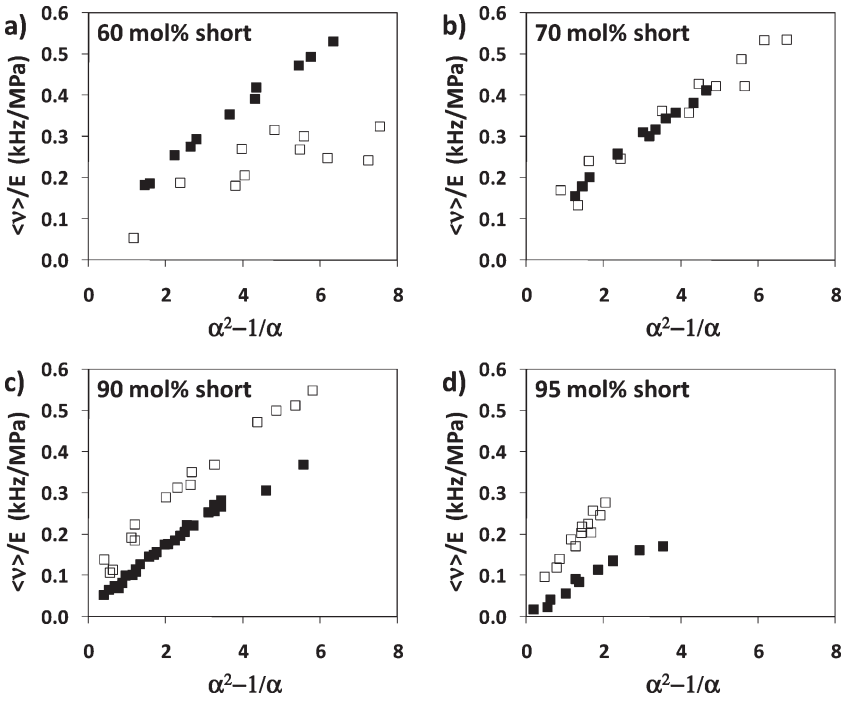

Figure 5. Average segmental order $\langle \nu \rangle$ normalized by elastic modulus E for short (open squares) and long (filled squares) chain segments in (a) 60, (b) 70, (c) 90, and (d) 95 mol % short-chain bimodal networks. The segment orientation of the short chains increases relative to the long chains as the short-chain concentration is increased.

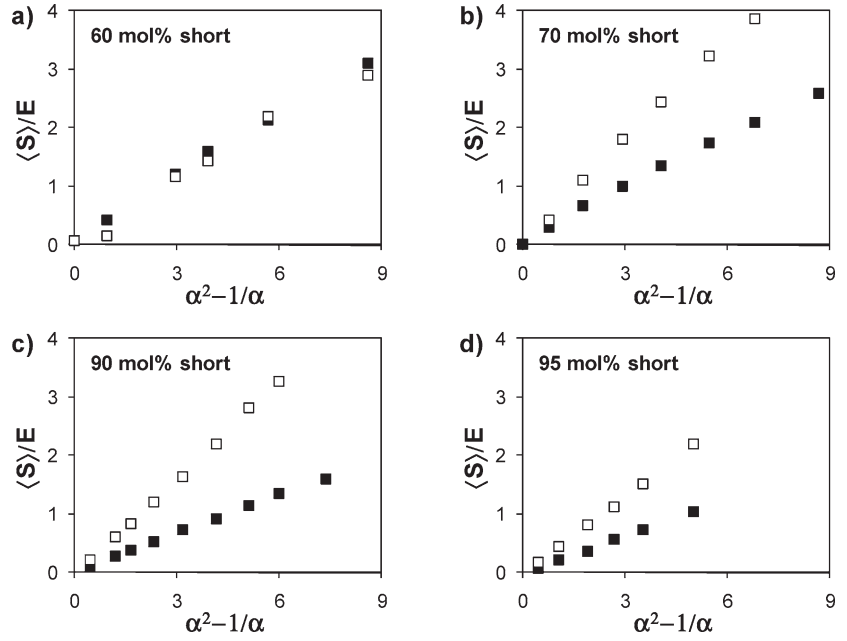

Figure 6. Average segmental order, $\langle S \rangle$, normalized by the dimensionless elastic modulus, E (in $k_B T/\sigma_{LJ}{}^3$ units), from molecular simulations of bimodal networks. Averages order parameters shown for short (open squares) and long (filled squares) chain segments in networks with (a) 60, (b) 70, (c) 90, and (d) 95 mol % of short chains.

Thus, the limited extensibility of the 90−95 mol % short chains must be the primary cause of the improved mechanical properties. While $\langle \nu \rangle$ is not a direct measure of end-to-end distance, the prominent spectral wings in the 90 mol % network (Figure 3) suggest that a significant portion of the orientation is due to segments on chains that are highly stretched by the movement of the cross-links. In fact, MC simulations have indicated that short-chain end-to-end distances in 90 mol % networks increase markedly with uniaxial elongation as compared to those in 60 mol % short-chain networks.[29] Increased residual order upon cross-linking for the short chains in the 90 and 95 mol % networks (Figures 1a, 2) predisposes some of these chain segments to a highly aligned state upon stretching.

While these results suggest that the extensibility of the short chains is a key factor in the enhanced mechanical properties of bimodal networks, we note that MC simulations have predicted that some degree of topological heterogeneity is likely at compositions around 90 mol % short chains.[29] Additionally, the overall order parameter distribution in 800−47 000 g/mol networks measured by MQ-NMR has a bimodal character up to relatively high short-chain

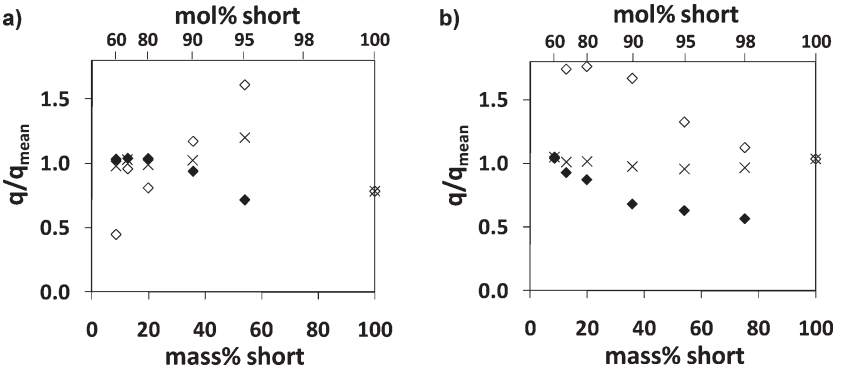

Figure 7. (a) Relative slopes of $\langle\nu\rangle/E$ vs $\alpha^2 - 1/\alpha = q$ at various bimodal compositions of PDMS networks and (b) relative slopes of $\langle S\rangle/E$ vs $\alpha^2 - 1/\alpha = q$ at various bimodal compositions of simulated networks. Values of relative q shown for short (open diamonds) and long (filled diamonds) chain segments. The mass % weighted average slope, q_{ave}, at each composition (x) is also displayed. All shown values are relative to q_{mean}, defined as the mean q_{ave} of the entire set of bimodal networks. For (a) $q_{mean} = 69.5$ Hz/MPa, and for (b) $q_{mean} = 0.327$ in σ_{LJ}^3/k_BT units.

concentrations, suggesting a slightly heterogeneous structure.[7,25] Thus, while relatively concentrated short chains in a 90 mol % network will not form small clusters, there are likely regions within such networks with higher cross-link densities. At this bimodal network composition, pockets with larger concentrations of long chains interspersed among the overall stiffer matrix would likely provide ductility. Such a structure might explain why the 90 mol % short-chain network (Figure 5c) could be stretched to nearly the same elongation at fracture as the 60 or 70 mol % networks (Figures 5a and 5b) even with the associated increase in cross-link density.

Classical rubber elasticity theories[32,42] predict that the average order parameter $\langle S\rangle$ is directly proportional to $E(\alpha^2 - 1/\alpha)$. Because $\langle\nu\rangle$ is a measure of $\langle S\rangle$, plots of $\langle\nu\rangle/E$ vs $\alpha^2 - 1/\alpha$ should follow a universal trend. Defining the slope of this line as q and taking the best fit line through our data, it seems from Table 1 that this universal relationship does not hold for our unimodal networks. This is unlike the previously reported $\Delta\nu/E$ vs $\alpha^2 - 1/\alpha$ data that follow the expected trend rather well,[13] but $\Delta\nu/E$ quantifies solely the contribution to segment orientation that arises from excluded volume interactions between neighboring segments.[13,38,26] It is also important to mention that the universal trend predicted by such classical theories is obtained for simulated unimodal networks (see Table 2). The average q for unimodal networks listed in Table 1 is calculated to be 80 ± 24 Hz/MPa, whereas the average q for the simulated unimodal networks shown in Table 2 is 0.345 ± 0.008 (in σ_{LJ}^3/k_BT units). The reason the theoretically predicted trend holds for the simulated unimodal networks, and not for experimental unimodal samples, may be attributed to the fact that the amount of inelastic (i.e., single-looped and pendant) chains in all simulated unimodal networks is relatively similar (Table 2). This similarity in the amount of inelastic material is not possible to achieve in all the PDMS unimodal samples.

As detailed in Figures 5 and 6, there is a clear redistribution of chain segment orientation with short-chain concentration. Figure 7 nicely quantifies this redistribution by displaying plots of relative values of the slope q vs mass (and mol) % of short chains for both PDMS and simulated bimodal networks. Computation of the weighted average q, q_{ave}, for each bimodal network is then performed by weighting the slopes for both the short and long chains (Figure 5) by their respective mass fractions within each network[27] (i.e., $q_{ave} = (\text{mass }\%_{short})q_{short} + (\text{mass }\%_{long})q_{long}$). Contrary to the results obtained from the set of PDMS unimodal networks and in agreement with classical theories, the studied set of both experimental and simulated bimodal networks (Figures 7a and 7b) seem to exhibit the above-mentioned universal trend. This is because the weighted averages q_{ave} remain relatively constant over different network compositions. The q_{ave} values yield a rather consistent mean value of $q_{mean} = (\langle\nu\rangle/E)/(\alpha^2 - 1/\alpha) = 69.5 \pm 9$ Hz/MPa for PDMS bimodal networks and $q_{mean} = (\langle S\rangle/E)/(\alpha^2 - 1/\alpha) = 0.327 \pm 0.012$ (in σ_{LJ}^3/k_BT units) for the simulated bimodal networks. These two mean average values q_{mean} are used as normalizing constants in Figures 7a and 7b, respectively.

Comparison of Figure 7a with 7b reveals evident qualitative discrepancies in the dependence of q/q_{mean} on the short-chain content for the short chains in PDMS and simulated bimodal networks. Such qualitative differences are due to the more perfect networks achieved in the simulations (e.g., the almost stoichiometric end-linking concentrations used and the significantly lower sol fractions obtained). Moreover, these qualitative discrepancies were somewhat expected because they are equivalent to those mentioned earlier when contrasting segment orientation trends in Figures 5 and 6. Thus, the corresponding previous discussion about those disparities also addresses the disparities found in Figures 7a and 7b.

3.3. ^{2}H NMR Line Shapes of Highly Stretched Networks. We recently reported on ^{2}H NMR line shapes for a series of unimodal networks.[28] At high extension, the 36 000 g/mol network spectra displayed a prominent shoulder in addition to the expected spectral splitting (Figure 8b). The line shapes were empirically fit to two pairs of doublets with splittings $\Delta\nu_w$ (outer or wide) and $\Delta\nu_n$ (inner or narrow) to describe the separation between the shoulders and the peak maxima, respectively.[28] This $\Delta\nu_n$ was shown to be equivalent to the $\Delta\nu$ reported in all previous ^{2}H NMR studies. We attributed the wide or outer splitting to the alignment of chain segments that are highly influenced by the cross-link constraints, while the narrow or inner splitting is thought to result from excluded volume interactions between segments of chains not very extended.[28] Two populations are also observed in the ^{2}H NMR spectra for labeled 90 000 g/mol chains in highly extended bimodal networks (Figure 8a). The spectrum line shapes of certain simulated unimodal (Figure 8d) and bimodal (Figure 8e) networks exhibit also a peculiar noticeable shoulder when highly stretched.

To explore the nature of those "two apparently different subpopulations" of chain segments that yield the two pairs of doublets in the ^{2}H NMR spectra, we use molecular simulations to examine in detail how chain segments can be separated into groups depending upon the degree of chain extension and overall chain orientation. Certainly, chain segments could be classified in more than two groups or even in a

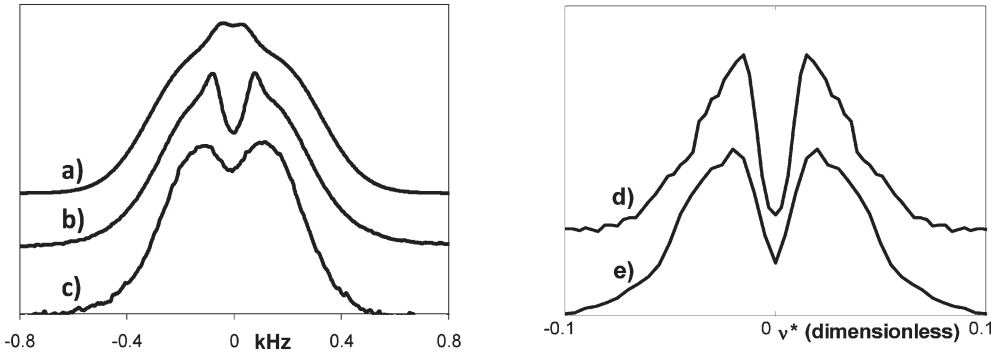

Figure 8. Experimental ^{2}H NMR line shapes for (a) 60 mol % short-chain bimodal network with ^{2}H-labeled long chains ($\alpha = 2.04$), (b) 36 000 g/mol unimodal network ($\alpha = 1.98$), and (c) 90 000 g/mol unimodal network ($\alpha = 2.26$). Simulated ^{2}H NMR line shapes for (d) 129-bead unimodal network ($\alpha = 3.05$) and (e) 90 mol % short-chain bimodal network with long (300-bead) chains labeled ($\alpha = 2.53$). For simulated networks, $\langle \nu^* \rangle$ is equal to $\langle S \rangle$.

continuum spectrum of populations. We limit our analysis to only a few groups (specifically two) of chains, as suggested by previous simulation[38] and empirical[28] approaches, because this appears to be sufficient to describe the origin of those singular shoulders in the spectra line shapes of highly extended networks.

We argue that the outer population corresponds to segments of relatively long chains that are able to be greatly stretched and extremely oriented toward the strain axis. Therefore, such chains may not interact extensively with other chains through entanglements. In addition, the cross-links at the end of those chains could significantly displace along the deformation axis. Because of their lack of interchain interactions, these highly stretchable chains may mostly undergo desinterspersion upon network extension. Conversely, the inner population may be regarded as segments of relatively long chains that are subject to more interchain interactions (i.e., trapped entanglements); consequently, these chains are weakly to moderately oriented toward the strain axis upon large extensions.

To quantify the extent of overall chain orientation (rather than segment orientation) along the extension axis in simulated networks, we define the average chain orientation order parameter Z as the second Legendre polynomial of the ratio of the chain mean-squared radius of gyration component along the strain axis ("z" direction) $R_{G,Z}^2$ to the total chain mean-squared radius of gyration R_G^2. The order parameter Z is then given by

$$Z = \frac{3R_{G,z}^2/R_G^2 - 1}{2} \tag{3}$$

Values of Z range from $-1/2$ (when all segments of a chain lie on a plane perpendicular to the "z" axis) to 1 (all segments of a chain are completely aligned parallel to the "z" axis). If chain segments are isotropically distributed, e.g., chains with random coil configurations, Z is equal to 0. A sketch of how Z is related to the overall orientation of the chain is displayed at the bottom right corner of Figure 9. This figure also shows the total dimensionless stress versus the ensemble average of Z in several simulated unimodal networks made with different chain lengths. Relatively large values of $\langle Z \rangle$, e.g., greater than 4/5, obtained for reasonable stresses (less than 0.15 in k_BT/σ_{LJ}^3 units) are only observed in networks with rather long chains. As an example of extreme chain alignment to the strain axis, chains with average Z values greater than 4/5 would exhibit average ellipsoidal-coil conformations with aspect ratios (i.e., $(\langle R_{G,Z}^2 \rangle / \langle R_{G,Y}^2 \rangle)^{1/2}$) greater than 3.6.

Large values of Z (i.e., greater than 4/5) are not observed for shorter chains (less than 100-bead long) because they

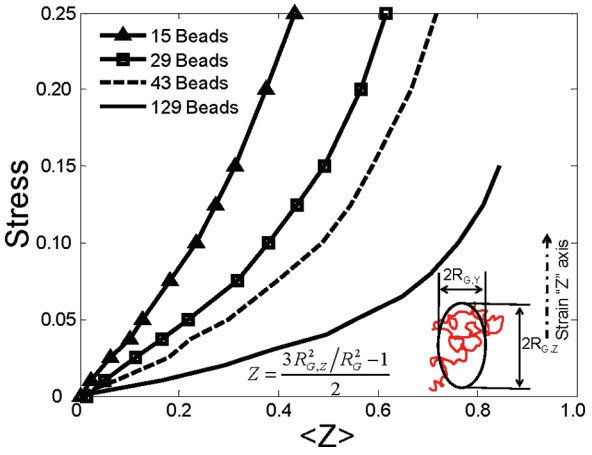

Figure 9. Stress (in k_BT/σ_{LJ}^3 units) vs average chain orientation order parameter $\langle Z \rangle$ (dimensionless) for various simulated unimodal networks with different chain lengths: 15-bead long (triangles), 29-bead long (squares), 43-bead long (dashed), and 129-bead long (solid line). At the bottom, the definition of Z and a sketch that illustrates the relation of Z to the average chain orientation.

would need to lose most of their configurational entropy to achieve such extremely oriented states. On the other hand, relatively long chains (longer than 100 beads) that lack entanglements with other chains need to lose only a part of their entropy in order to attain such aligned configurations. This could explain why the unusual shoulders in line shapes are only seen for segments of PDMS chains with relatively high molar masses (e.g., greater than 36 000 g/mol[28] that are roughly equivalent to chain lengths of 120 beads in our simulated networks).

Using this order parameter Z of overall chain orientation, we decompose the simulated spectrum of long chains (300-bead) in a highly extended bimodal network (also displayed in Figure 8e) into two spectra: one corresponding to weakly or moderately oriented long chains (with $\langle Z \rangle < 4/5$) and another to exceptionally oriented long chains (with $\langle Z \rangle > 4/5$). Such decomposition (Figure 10) clearly shows that the outer shoulder (or wide splitting) arises from segments belonging to long chains that are extremely oriented and deformed toward the strain axis. The inner segment population (or narrow splitting), however, corresponds to segments of long chains that are moderately or even weakly oriented and deformed along the extension direction. Thus, the empirical approach used in ref 28 to analyze this type of complex line shapes exhibiting two pair of doublets may be seen as phenomenologically correct. This empirical analysis could, for instance, be employed to gain insights about the relative

sizes of these "two" chain segment populations through comparisons between the areas under the spectra of the outer and inner splittings. Moreover, this information about these two groups of long chains with different orientational responses may also be related to the network tensile properties, such as modulus, ultimate strain, and toughness.

We proceed now to analyze and compare the complex spectra observed for rather long chains in PDMS unimodal and bimodal networks through the approach used in ref 28. While the shoulders are not always as pronounced in these systems as in the 36 000 g/mol unimodal network, all the PDMS bimodal long-chain line shapes were successfully fit to doublets with peak separation $\Delta\nu_w$ and $\Delta\nu_n$. These data are normalized by the elastic modulus and plotted vs $\alpha^2 - 1/\alpha$ in Figure 11a. Values of $\Delta\nu$/E fall in the range predicted by ideal elasticity theory, $0.2\omega_Q a^3/k_B T \cong 0.14 \times 10^{-3}$ Hz/Pa, with $\omega_Q \cong 250$ kHz/12 = 21 kHz (taking local rotations into account) and $a^3 \cong (0.52\ \text{nm})^3$. The $\Delta\nu_w/E$ and $\Delta\nu_n/E$ data follow universal trends for both unimodal and bimodal networks across different precursor chain lengths and compositions. This correspondence indicates that the effects of the excluded volume interactions and the constraints on segmental alignment are each linked to the average mesh size (modulus) of the bulk network. Therefore, it is surprising that the 90 000 g/mol unimodal network line shape does not display a shoulder (Figure 8c), even though the long chains in bimodal networks employed in this study (depicted in Figure 8a) are of the same precursor molar mass. The splitting between the peak maxima for the 90 000 g/mol unimodal network are plotted in Figure 11b against best-fit lines generated from the unimodal and bimodal network data in Figure 11a. Also included are previously published data[28] for ^{2}H-labeled 30 000 g/mol free chains dissolved in a protonated host network. Because these probe chains are not chemically attached to the network, their segments only align through excluded volume interactions with neighboring chains. These data follow the $\Delta\nu_n/E$ trend line as expected. Meanwhile, the $\Delta\nu$ values for the 90 000 g/mol network closely follow the $\Delta\nu_w/E$ relationship associated with segment alignment due to the effect of constraints. Thus, in Figure 8c the inner doublet $\Delta\nu_n$ is concealed by a more prominent outer doublet $\Delta\nu_w$ caused by segments of chains that are highly aligned due to the effect of cross-links and lack of entanglements. We attribute this line shape characteristic to the structure of the 90 000 g/mol unimodal network. This network was the only sample tested that could be classified as "nonmodel" due to its large soluble fraction and high degree of swelling in toluene (w_{sol} = 5.48%, Q = 7.31; Table 1). The 90 000 g/mol chains in bimodal networks are incorporated into networks of significantly better quality (Table 1) due to the associated increase in cross-link density. The molar mass between effective junctions, which takes into account the presence of trapped entanglements along the elastic chains, can be calculated from

$$M_c = 3\rho RT/E \tag{4}$$

Taking ρ = 0.97 g/cm^3 for PDMS and elastic modulus values from Table 1, we calculate M_c = 27 000 and 12 000 g/mol for the unimodal networks synthesized from 90 000 and 36 000 g/mol precursors, respectively. Therefore, elastic chains in both networks are expected to have about two effective junctions along their chain lengths, even though the 90 000 g/mol chains are almost 3 times longer than the 36 000 g/mol chains. The lack of a visible "moderately or weakly oriented chain" split $\Delta\nu_n$ can then be explained by the relative reduction of interchain interactions in the longer chain unimodal network. We suspect that the presence of pendant chains and the removal of the relatively high fraction of soluble chains upon extraction led to chain interspersion (nontrapped entanglements).[43,44] Upon uniaxial extension the chains primarily disintersperse,[45] diminishing the effect of excluded volume interactions. Consequently, the segment alignment is dominated by the movement of the cross-links. This effect appears to have eclipsed the contribution of chain segment interactions between pendant chains and the elastic

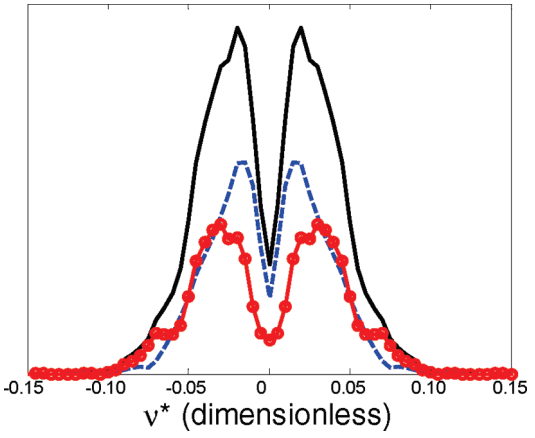

Figure 10. ^{2}H NMR simulated line shape for the 90 mol % short chain bimodal network with long chains labeled (solid line) as well as its decomposition into spectra yielded by weakly to moderately (dashed line) and highly (circles) oriented long chains. Chains with $\langle Z\rangle > 4/5$ are considered greatly oriented; otherwise, they are considered to be weakly to moderately oriented. Elongation ratio α = 2.53. $\langle\nu^*\rangle$ is equal to $\langle S\rangle$.

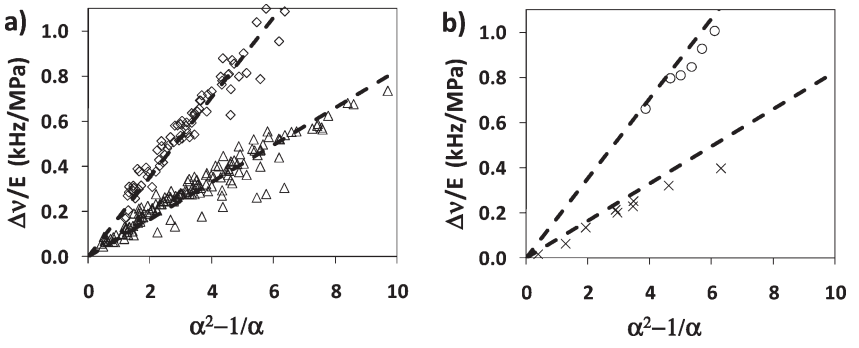

Figure 11. (a) All data for the narrow ($\Delta\nu_n/E$, triangles) and wide ($\Delta\nu_w/E$, diamonds) spectral splittings found in ^{2}H NMR line shapes of unimodal and bimodal networks and the best-fit lines through these data. (b) $\Delta\nu/E$ for the 90 000 g/mol unimodal network (circles) and the 30 000 g/mol ^{2}H-labeled free chains dissolved in a protonated 30 000 g/mol network (×) plotted against the best-fit lines generated in (a).

network because an increased fraction of pendant chains is expected in such nonmodel networks.[30] The relative lack of $\Delta\nu_n$ in the 90 000 g/mol unimodal network causes it to show a higher degree of average segmental orientation with respect to elastic modulus than the other unimodal networks (Table 1). This effect is also demonstrated by the 36 000 g/mol precursors reacted in the presence of 30% nonreactive chains. After the solvent chains are extracted, this network (36 000d) shows a higher degree of segment orientation than the standard 36 000 g/mol unimodal network. We expect a higher contribution from disinterspersion of chains in the 36 000d network due to its collapsed structure upon extraction. Table 1 also indicates a higher value of q for this network before removal of solvent chains (80.6 Hz/MPa) than after (73.3 Hz/MPa). This difference results from the decreased degree of intersegmental interactions between network chains when solvent chains are present.[43,44]

4. Conclusions

Segmental ordering in bimodal networks is investigated using ^{2}H NMR spectroscopy. We calculate the average absolute value $\langle|\nu|\rangle$ of the spectra to confirm the presence of highly oriented segments. Estimates of the total average chain segment order $\langle\nu\rangle$ are obtained from the entire ^{2}H NMR spectrum through a recently developed methodology.[27] Even in the rest state, the line shapes of the short- and long-chain components are markedly different due to the different degrees of motional restriction on each. These spectral shapes are qualitatively reproduced in MC molecular simulations. The conformation of long chains is not affected when they are incorporated into a bimodal network structure. However, $\langle|\nu|\rangle_0$ values for short chains in undeformed networks evolve with bimodal composition as a result of the network topology.

Networks at about 90 mol % are of particular interest because they have been demonstrated to produce optimal mechanical properties. Here, the high $\langle|\nu|\rangle_0$ value indicates increased motional restriction on the short chains that is likely the result of chains with a relatively high end-to-end distance during network formation. We further connect microstructure and macroscopic properties by measuring ^{2}H NMR spectra for samples that have been uniaxially stretched. These experiments and results from the corresponding coarse-grained molecular simulations clearly demonstrate the reapportionment of segmental orientation from long to short chains with increasing short-chain concentration. When their concentration is at 60 mol %, the shorter chains are found to be protected from segmental alignment since they are clustered into small domains within a medium of longer chains. Here, the segmental orientation of the shorter chains is dominated by excluded volume interactions between neighboring chains.

Optimum mechanical properties found with 90 mol % short chains are primarily due to increased mechanical loading on the short chain matrix. Wide spectral wings for these ^{2}H-labeled short chains indicate that some of these chains are moderately stretched even at the unperturbed state. The segmental alignment of the short chains is at a maximum when their concentration is further increased, but the networks become increasingly brittle. Thus, the ductility afforded by the long-chain component is essential to producing bimodal networks with enhanced mechanical properties. There are likely regions dominated by long chains within these optimal networks that allow the samples to stretch without fracture even as the short chains are increasingly loaded. Although the relative orientation of short- and long-chain segments clearly evolves with concentration, both experiments and molecular simulations indicate that the overall segmental alignment normalized by the elastic modulus is equal across all bimodal network compositions.

Through molecular simulations we further explored the microstructural nature of atypical ^{2}H NMR spectra of highly extended unimodal and bimodal samples exhibiting two characteristic quadrupolar splittings. The outer splitting corresponds to segments of rather long chains that are able to be greatly stretched and oriented toward the strain axis. Conversely, the inner frequency splitting may be attributed to segments of chains that undergo more interchain interactions (i.e., trapped entanglements); as a result, these chains are moderately or even weakly oriented toward the strain axis.

Acknowledgment. This work was supported by the National Science Foundation Polymers Program under Grant DMR-0705565.

References and Notes

(1) Mark, J. E. *J. Phys. Chem. B* **2003**, *107*, 903–913.
(2) Andrady, A. L.; Llorente, M. A.; Mark, J. E. *J. Chem. Phys.* **1980**, *72*, 2282.
(3) Wu, W. L.; Jong, L.; Hanyu, A.; Coynse, L. D.; Stein, R. S. *Macromolecules* **1990**, *23*, 351–353.
(4) Smith, T. L.; Haidar, B.; Hedrick, J. L. *Rubber Chem. Technol.* **1990**, *63*, 256.
(5) Oikawa, H. *Polymer* **1992**, *33*, 1116–1119.
(6) Hecht, A.; Horkay, F.; Geissler, E. *J. Phys. Chem. B* **2001**, *105*, 5637–5642.
(7) Saalwächter, K.; Ziegler, P.; Spyckerelle, O.; Haidar, B.; Vidal, A.; Sommer, J. *J. Chem. Phys.* **2003**, *119*, 3468–3482.
(8) Llorente, M. A.; Andrady, A. L.; Mark, J. E. *J. Polym. Sci., Polym. Phys.* **1981**, *19*, 621–630.
(9) Mark, J. E.; Tang, M. *J. Polym. Sci., Polym. Phys.* **1984**, *22*, 1849–1855.
(10) Mark, J. E. *Acc. Chem. Res.* **1994**, *27*, 271–278.
(11) Sotta, P.; Deloche, B. *Macromolecules* **1990**, *23*, 1999–2007.
(12) Brereton, M. G. *Macromolecules* **1993**, *26*, 1152–1157.
(13) McLoughlin, K.; Waldbieser, J. K.; Cohen, C.; Duncan, T. M. *Macromolecules* **1997**, *30*, 1044–1052.
(14) Warner, M.; Callaghan, P. T.; Samulski, E. T. *Macromolecules* **1997**, *30*, 4733–4736.
(15) Chapellier, B.; Deloche, B.; Oeser, R. *Prog. Colloid Polym. Sci.* **1992**, *90*, 111–114.
(16) Chapellier, B.; Deloche, B.; Oeser, R. *J. Phys. II* **1993**, *3*, 1619–1631.
(17) Sotta, P. *Macromolecules* **1998**, *31*, 3872–3879.
(18) Galiatsatos, V.; Mark, J. E. *Macromolecules* **1987**, *20*, 2631–2632.
(19) Subramanian, P. R.; Galiatsatos, V. *Makromol. Chem., Macromol. Symp.* **1993**, *76*, 233.
(20) Viers, B.; Mark, J. *J. Inorg. Organomet. Polym. Mater.* **2007**, *17*, 283–288.
(21) Hanyu, A.; Stein, R. *Makromol. Chem., Macromol. Symp.* **1991**, *45*, 189–203.
(22) Besbes, S.; Bokobza, L.; Monnerie, L.; Bahar, I.; Erman, B. *Macromolecules* **1995**, *28*, 231–235.
(23) Sotta, P. *Macromolecules* **1998**, *31*, 8417–8422.
(24) Saalwächter, K. *J. Am. Chem. Soc.* **2003**, *125*, 14684–14685.
(25) Saalwächter, K.; Sommer, J. *Macromol. Rapid Commun.* **2007**, *28*, 1455–1465.
(26) Ries, M. E.; Brereton, M. G.; Klein, P. G.; Ward, I. M.; Ekanayake, P.; Menge, H.; Schneider, H. *Macromolecules* **1999**, *32*, 4961–4968.
(27) Aguilera-Mercado, B. M.; Cohen, C.; Escobedo, F. A. *Macromolecules* **2009**, *42*, 8889–8898.
(28) Genesky, G. D.; Duncan, T. M.; Cohen, C. *Macromolecules* **2009**, *42*, 8882–8888.
(29) Genesky, G. D.; Aguilera-Mercado, B. M.; Bhawe, D. M.; Escobedo, F. A.; Cohen, C. *Macromolecules* **2008**, *41*, 8231–8241.
(30) Patel, S. K.; Malone, S.; Cohen, C.; Gillmor, J. R.; Colby, R. H. *Macromolecules* **1992**, *25*, 5241–5251.
(31) Takahashi, H.; Shibayama, M.; Fujisawa, H.; Nomura, S. *Macromolecules* **1995**, *28*, 8824–8828.
(32) Flory, P. J. *Principles of Polymer Chemistry*; Cornell University Press: Ithaca, NY, 1953.
(33) Carmesin, I.; Kremer, K. *Macromolecules* **1988**, *21*, 2819.
(34) Paul, W.; Binder, K.; Heermann, D.; Kremer, K. *J. Phys. II* **1991**, *1*, 37.

(35) Binder, K.; Paul, W. *J. Polym. Sci., Polym. Phys*. **1997**, *35*, 1.
(36) Depner, M.; Deloche, B.; Sotta, P. *Macromolecules* **1994**, *27*, 5192–5199.
(37) Sotta, P.; Higgs, P. G.; Depner, M.; Deloche, B. *Macromolecules* **1995**, *28*, 7208–7214.
(38) Yong, C. W.; Higgs, P. G. *Macromolecules* **1999**, *32*, 5062–5071.
(39) Deloche, B.; Beltzung, M.; Herz, J. *J. Phys., Lett*. **1982**, *43*, L763–L769.
(40) Gronski, W.; Stadler, R.; Maldaner Jacobi, M. *Macromolecules* **1984**, *17*, 741–748.
(41) Trautenberg, H. L.; Sommer, J.-U.; Goritz, D. *Macromol. Symp*. **1994**, *81*, 153.
(42) Kuhn, W.; Grün, F. *Colloid Polym. Sci*. **1942**, *101*, 248–271.
(43) Sivasailam, K.; Cohen, C. *J. Rheol*. **2000**, *44*, 897–915.
(44) Urayama, K.; Kohjiya, S. *J. Chem. Phys*. **1996**, *104*, 3352.
(45) Urayama, K.; Kohjiya, S. *Polymer* **1997**, *38*, 955–962.